Gravitropically Stabilized Self-Assembly of Active Microcrystallites and Spinning Free Janus Particles

Seyed Amin Nabavizadeh, John Castañeda, John G. Gibbs,* and Amir Nourhani*

Active colloidal microcrystallites capable of generating flow patterns around or through their porous network are introduced, which in combination with "free microspheres," create self-assembled active clusters with multiple moving parts. Fluid flow draws microspheres within a microcrystallite's local environment toward—and aggregate at—the edge of the microcrystallite, where the previously translational movement transitions to continuous spinning. These experiments show that the spinning frequency decreases with an increase in diameter and that when the center of mass of a spinning particle is shifted off-center—here Janus spheres—a time-varying angular frequency is observed. Weight-anisotropy also leads to a particularly intriguing phenomenon, which manifests as the spontaneous realignment of the rotational axis to a preferential direction; this effect is attributed to a gravitropic self-correcting mechanism. Thus, the dynamics of the self-assembled active structure remains stable over long time periods, despite being subjected to significant noise, for example, Brownian forces.

1. Introduction

Experimental realization[1–6] and theoretical modeling[7–10] of individual self-propelling active microparticles—the active

S. A. Nabavizadeh, A. Nourhani
Department of Mechanical Engineering
University of Akron
Akron, OH 44325, USA
E-mail: nourhani@uakron.edu
J. Castañeda, J. G. Gibbs
Department of Applied Physics and Materials Science
Northern Arizona University
Flagstaff, AZ 86011, USA
E-mail: john.gibbs@nau.edu
J. Castañeda, J. G. Gibbs
Center for Materials Interfaces in Research and Applications
Northern Arizona University
Flagstaff, AZ 86011, USA
A. Nourhani
Biomimicry Research and Innovation Center
University of Akron
Akron, OH 44325, USA
A. Nourhani
Departments of Biology, Mathematics, and Chemical, Biomolecular, and Corrosion Engineering
University of Akron
Akron, OH 44325, USA

engine of autonomous micromachines—have undergone compelling and impressive progress in recent years, resulting from an aggressive campaign to advance this field. Major advancements include microrobots that are purely artificial,[11–16] biomimetic,[17,18] or biohybrid,[19–24] with other varieties in development. The path to realizing autonomous small-scale machinery has already engendered new research directions including fundamental insights into non-equilibrium phenomena[25,26] and has catalyzed the development of specialized applications at the microscale. [27–30]

Parallel developments have aimed at understanding and manipulating interactions between self-propelling colloids[31–37] and the interplay of powered motion and random phenomena.[38–41] The complexity and varieties of these effects potentially frustrate straightforward modeling of the dynamics, but this same complexity simultaneously opens up immense opportunities for designing systems with rich phenomenology. This has already been seen in the collective behavior that arises in dense suspensions of self-propelled, small-scale objects.[42–46] Despite these advances, continuing to move toward the ambitious goal of developing complex micromachinery requires research and design of new and improved autonomous microcomplexes, and an important next step is to develop self-assembling systems consisting of multiple independently moving parts. Furthermore, having those autonomous dynamical behaviors be regular and self-correcting, even in an evolving and noisy environment, is paramount to such advancements.

In this paper, we present a self-correcting, self-assembled autonomous microstructure with multiple dynamic parts made from an active, porous 2D colloidal network and spinning free particles, as shown in **Figure 1**. The 2D colloidal network has a triangular lattice structure and thus, we term it an "active microcrystallite" (see **Figure 2** and video V1, Supporting Information). The crystallite is a monolayer of silica (SiO$_2$) microbeads that are half-coated and interconnected by a layer of platinum (Pt). It serves as the engine of the systems such that hydrogen peroxide (H$_2$O$_2$) decomposes over the Pt surface, leading to a flow-field generated around and through the microcrystallite toward the Pt side. This flow drags free particles in the local environment toward the 2D active microstructure's edge. Once assembled at the edge, the free particles' translational mode of motion changes to continuous spinning. We have corroborated this mechanism for

**ADVANCED
SCIENCE NEWS**
www.advancedsciencenews.com

Particle
& Particle Systems Characterization
www.particle-journal.com

Figure 1. a) The flow generated by an active microcrystallite drags nearby free particles to its edge where the mode of motion transitions from translation to spinning. b) The spinning rate of a free Janus particle varies over one period of rotation and depends on the instantaneous orientation of the particle.

experimental observations with multiphysics simulations and theoretical modeling.

Additionally, we investigate a self-aligning effect exhibited by the spinning Janus microspheres. More specifically, we demonstrate that the combination of fluid being pumped toward and through the crystallite and importantly, the Janus spheres' anisotropic weight distribution conspire to give rise to two primary effects: 1) The spinning frequency is nearly constant over long times, but the angular frequency varies with regular periodicity over short time-frames; 2) the orientation of the spinning axis has a preferred perpendicular direction with respect to the director of the Janus sphere. The combination of these effects allows the active crystallites and free spinning particle to become de facto complex microstructures made from multiple independently moving parts that are autonomous, self-assembled, and inherently stable. This self-correcting dynamics is observed even when the spinning particles are subjected to significant noise or other destabilizing forces.

2. Results and Discussion

The building blocks of an active crystallite are SiO_2 microspheres half-coated with Pt. Single bi-faceted Janus microspheres are an archetype of catalytic microswimmers in a hydrogen peroxide (H_2O_2) solution.[41] The catalytic decomposition of H_2O_2 results

in fluid flow from the SiO_2 to the Pt (in the particle reference frame), which gives rise to particle motion toward its SiO_2 side (in the laboratory reference frame). Active crystallites are effectively interconnected and aligned Janus particles, as illustrated in Figure 2a. While they have a similar constitution and operating fluid dynamics mechanism to the single Janus spheres, active crystallites provide richer dynamics in terms of fluid flow and interaction with other objects—free particles—in the vicinity. As the natural axes of the aligned Janus spheres in a crystallite—pointing from the pole of one hemispherical face to the other—are oriented mutually perpendicular to the crystal plane, they generate flow patterns that are significantly more structured in comparisons to flows created by aggregates of randomly oriented individual Pt/SiO_2 microswimmers.[37] To fabricate crystallites, we exploit the same physical vapor deposition process that can be used for creating individual Janus spheres,[47] with the only difference being a substantially thicker layer of deposited Pt onto a triangular lattice of microspheres monolayer. During the fabrication, the deposition of Pt is continued until the metal forms a "bridge" that permanently bonds adjacent spheres, as shown in Figure 2a. The Pt thickness required for creating bridges depends upon the microsphere diameter, the details of which are beyond the scope of the current work.

The crystallites settle in water under the influence of gravity. When activated by H_2O_2, a crystallite orients parallel to the bottom substrate with the Pt face pointing upward (Figure 2b). Moreover, free particles in the vicinity are dragged toward the crystallite until eventually reaching the edge. To improve our ability to investigate the flow-dynamics, we used individual Janus spheres consisting of silica or polystyrene microspheres half-coated with a noble metal such as gold (Au) or titanium dioxide (TiO_2), as shown in Figure 2b. More specifically, we use noble-metal-coated Janus spheres as the metal coating is reflective, allowing convenient observation of the rotational dynamics. Among the noble metals (Au, Pd, Rh) in our study, only the reaction rate of H_2O_2 for Au is small enough such that an Au-coated particle does not create a strong enough flow field for self-propulsion. Even though we would anticipate that the possibility for the self-propulsion of the free Janus particles made of Pd or Rh may add to the complexity of the experiment and resulting competing flows, as we elaborate soon, the difference in the activity of noble metals has minimal effect on spinning rate. Moreover, we did not observe any detachment of free self-propelling Janus particles after gathering at the edge of the microcrystallites. After the free Janus spheres assemble at the edge of an active crystallite, the former remain free to spin continuously—in most cases—with a regularity that can be observed directly; that is, simply looking at the behavior captured in the raw video data suggests stable dynamics (see Figure 2c; Video V1, Supporting Information).

While optical contrast between the two halves of a Janus sphere enables the observation of the spinning particle's angular orientation, our initial observations raised the question of whether the particles were spinning in a single direction, or oscillating back and forth. To address this question, we constructed Janus spheres from fluorescently dyed polystyrene (Figure 2d,e); fluorescence, combined with the opacity of the shell, drastically improves one's ability to visualize clearly

ADVANCED
SCIENCE NEWS
www.advancedsciencenews.com

Particle
& Particle Systems Characterization
www.particle-journal.com
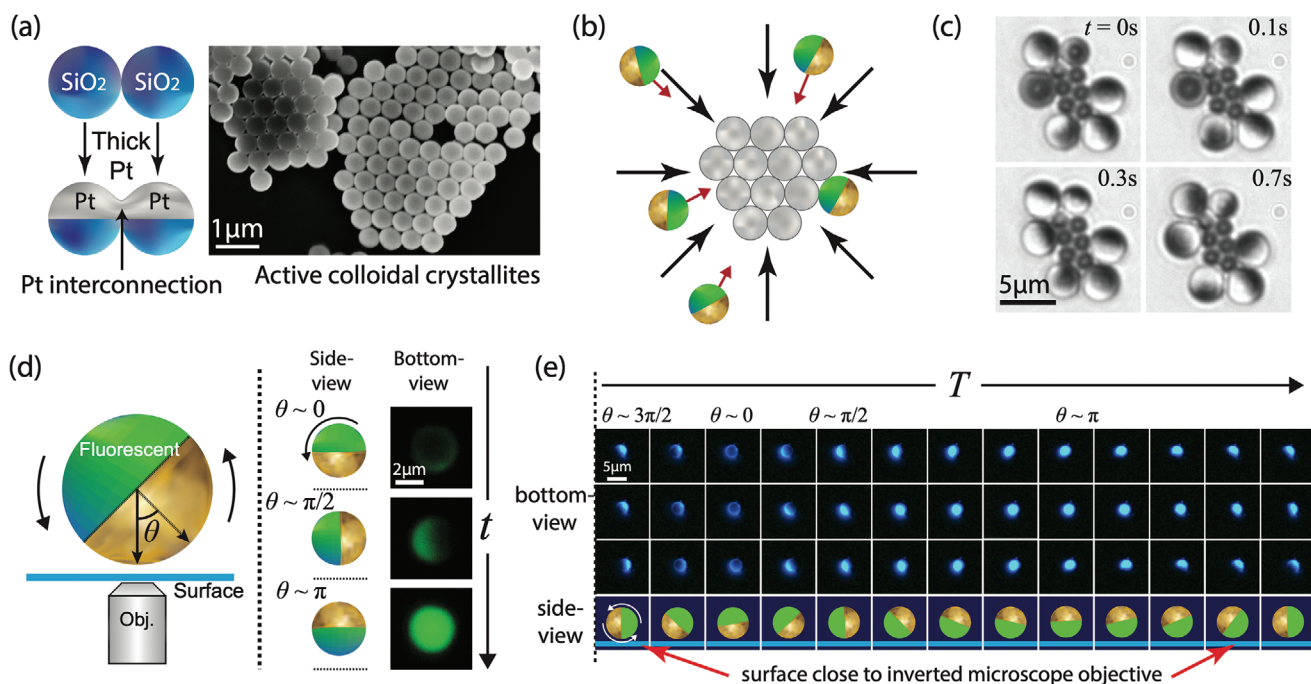
Figure 2. a) Fabrication of a crystallite by depositing a thick layer of Pt for inter-particle bonding, with an scanning electron microscopy (SEM) image of the resulting structures. b) Free Janus spheres are dragged toward an activated microcrystallite by the flow field in H_2O_2 solution. c) Video frames demonstrate several Janus spheres spinning at the edge of an active crystallite. In this example, the diameter of the spinning particles is greater than the diameter of the spheres making up the crystallite. d) Fluorescent Janus spheres reveal the full rotational behavior. e) Time-series of video frames showing the different phases of rotation with side-view schematic representations of the corresponding phases on the bottom row.

the particle's orientation and spinning dynamics: Described in simple terms, this experiment shows that the Janus spheres rotate end-over-end. This observation forms the foundation of our model: The continuous regular spinning is the result of coupling of multiple effects including the flow pattern generated by the crystallite and the weight anisotropy from the heavy metal cap.

The free particles spin such that their symmetry plane is perpendicular to the crystallite plane, and thus we can characterize the state of the particle for a majority of freely spinning Janus particles by a single metric, θ, defined in the schematic of Figure 2d. The microscope objective is underneath the sample and therefore most of the fluorescent light is blocked when the opaque coating is positioned downward, toward the objective. We arbitrarily choose this orientation to be $\theta = 0°$; two other example angles are shown in Figure 2d as well. A series of frames illustrating three complete rotations of a single Janus microsphere is also presented in Figure 2e. The adjacent columns are spaced equally in time, and each row corresponds to a single, complete rotation with a period T. The regularity of the rotational motion is illustrated by how the particle is in approximately the same phase in all three frames of any given column.

Our hypothesis—that the mechanism for the observed spinning motion at a crystallite's edge results from fluid flow toward and through the active network—is supported and confirmed experimentally and by multiphysics simulations. Further verification of the flow dynamics could in principle be investigated by direct visualization, but this is beyond the scope of the current project and our current experimental capabilities. Thus, we took an implicit route. We altered several experimental

parameters, summarized in **Figure 3**, in order to investigate this hypothesis inspired by the known behavior of a single Janus sphere.[48] Our hypothesis is supported by the observation of the following two effects: 1) With an increase in H_2O_2 concentration, the average flow speed $\bar{v}$ increases, and, thus, so should the average angular frequency $\bar{\omega} = 2\pi/T$, where T is the period of full rotation; 2) with greater Janus sphere diameter D, the average angular speed $\bar{\omega} \propto \bar{v}/D$ should decrease. These two effects are confirmed in Figures 3a and 3b, respectively.

Our next step was to investigate the effect of free-particle composition on the rotational dynamics. We considered the possibility that the spinning behavior could be affected by different factors beyond the already mentioned fluid flow toward a crystallite including particle-surface interactions, which change as a function of material, and the surface catalytic activity. To help untangle these effects and to better clarify the dominant factor, we examined free Janus particles with several material-compositions. The average spinning frequency as a function of material is given in Figure 3c; note that the size of the particles and the concentration of H_2O_2 are held constant as a means to independently check the effect of material alone. The decomposition rate of hydrogen peroxide over the coated hemispherical shell follows the sequence $TiO_2 < Au < Rh < Pd$, such that the rate constant for rhodium is one order of magnitude more than gold.[49] However, angular speeds reported in Figure 3c follow the sequence $TiO_2 < Au < Pd < Rh$; furthermore, the angular speeds are numerically close and safely of the same order of magnitude. Although it is possible that the data does in fact show some material-dependent differences in $\bar{\omega}$, note that the differences are not statistically significant (see errors
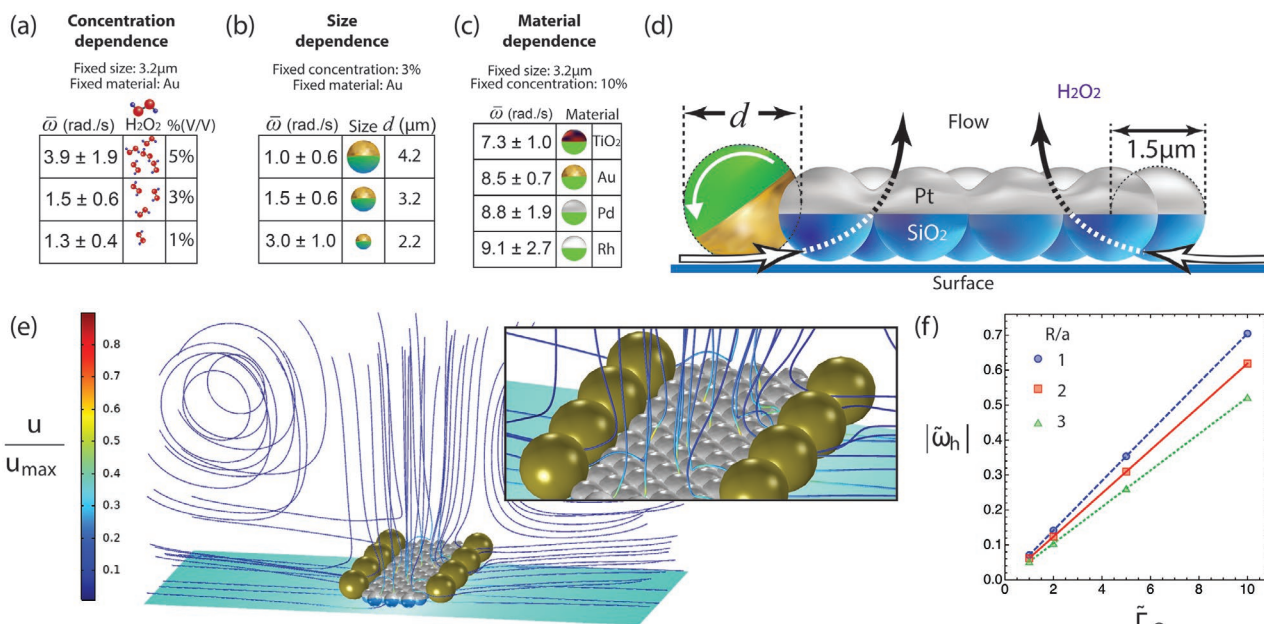
Figure 3. Experimental data for spinning dynamics together with multiphysics simulations suggest the primary effect of the observed dynamics arises from hydrodynamic fluid flow generated by the active crystallites. The average angular frequencies, $\bar{\omega}$, as a function of a) the concentration of H_2O_2, b) Janus particle diameter, d, and c) material from which the Janus spheres are made. d) Schematic representation of a single Janus sphere rotating adjacent to an active crystallite. The flow moves beneath and through the porous structure, dragging the bottom of the sphere toward the edge. e) Snapshots of our multiphysics simulations that corroborate the proposed flow field, as hypothesized based upon experimental data. f) The dependence of the dimensionless hydrodynamic-induced spinning rate upon the dimensionless surface flux for ratios of free particle radius R to the radius a of a particle in the microcrystallite for values $R/a = 1, 2, 3$.

reported for $\bar{\omega}$ in Figure 3c). Therefore, while the chemical composition may have some minor effects, the dominant factor leading to the torque that spins the particles appears to be the hydrodynamic effect due to flow toward and through the active crystallite, as previously discussed. The remainder of this paper is dedicated to analyzing this flow and its consequential effects upon the dynamics of the self-assembled microstructures.

A qualitative schematic illustration of our observations and conclusion so far is given in Figure 3d. The free Janus particle rotates such that its bottom spins toward the crystallite, consistent with the proposed flow direction generated by the active crystal. The crystallite is oriented with the Pt side opposite gravity, parallel to the surface above which the action takes place. The flow past the edges and through the porous structure pins the crystallite against the solid bottom surface. We did not observe the scenario of inverted orientation, in which case the SiO_2 face is instead upward. However, in such an orientation, we expect the fluid flow would be downward and the crystal would then be expected to self-propel away from the surface, against gravity, until eventually resettling into the stable configuration in Figure 3d. We did not observe the nucleation of bubbles on the microcrystallite surface and thus we attributed the Pt-upward orientation to the generated flow field.

We developed a minimal diffusiophoretic model to investigate the flow pattern generated by an active crystallite (explained in detail in Section 2). The model assumes the free particles are already aggregated around the edge of the microcrystallites, and thus phoretic interactions[50] are limited to slip velocities and possible contributions from density driven convective flow[51] are not taken into account for simplicity.

The spheres in the microcrystallite have radius a, and the diffusivity and far-field concentration of oxygen are $C_{O_2}^\infty$ and D_{O_2}, respectively. We model the phenomena by assigning non-zero surface flux Γ_{O_2} for oxygen over the Pt surface, and solve the Laplace equation for the concentration of oxygen. The spatial distribution of oxygen in solution is controlled by the dimensionless surface flux $\tilde{\Gamma}_{O_2} \equiv a\Gamma_{O_2}/(D_{O_2}C_{O_2}^\infty)$. Then, we calculate the slip velocity over the surfaces, and solve the Stokes equation to obtain the fluid pattern. The resulting flow pattern for the stable configuration is demonstrated in Figure 3e, which verifies the proposed hydrodynamic mechanism for spinning of free particles at the edge of the microcrystallite. Note that the free particles are isotropic in the simulation depicted in Figure 3e and thus the spinning rate ω_h due to hydrodynamic flow is time-independent. The fluid flows along the bottom substrate toward the crystal, which can drag particles with the fluid, thus accounting for the observed self-assembly in Figure 3e. The characteristic speed of the flow is $U^* = \mu_{ph}C_{O_2}^\infty/a$ where in our minimal model a uniform phoretic mobility μ_{ph} is considered over the surfaces. Our simulation results in Figure 3f show that the dimensionless spinning rate $\tilde{\omega}_h = \omega_h a/U^*$ due to hydrodynamic flow increases with greater dimensionless oxygen surface flux $\tilde{\Gamma}_{O_2}$, and decreases with larger free particle size R, as observed in our experiments. We next turn to the specific case of the Janus spheres acting as the free particles and their gravitropic behavior, as reported herein for our experimental results.

Tropism is the turning or growth of a biological organism in a specific direction in response to an external stimulus—for example, daisies and sunflowers turn toward the sun

**ADVANCED
SCIENCE NEWS**

www.advancedsciencenews.com

Particle
& Particle Systems Characterization

www.particle-journal.com
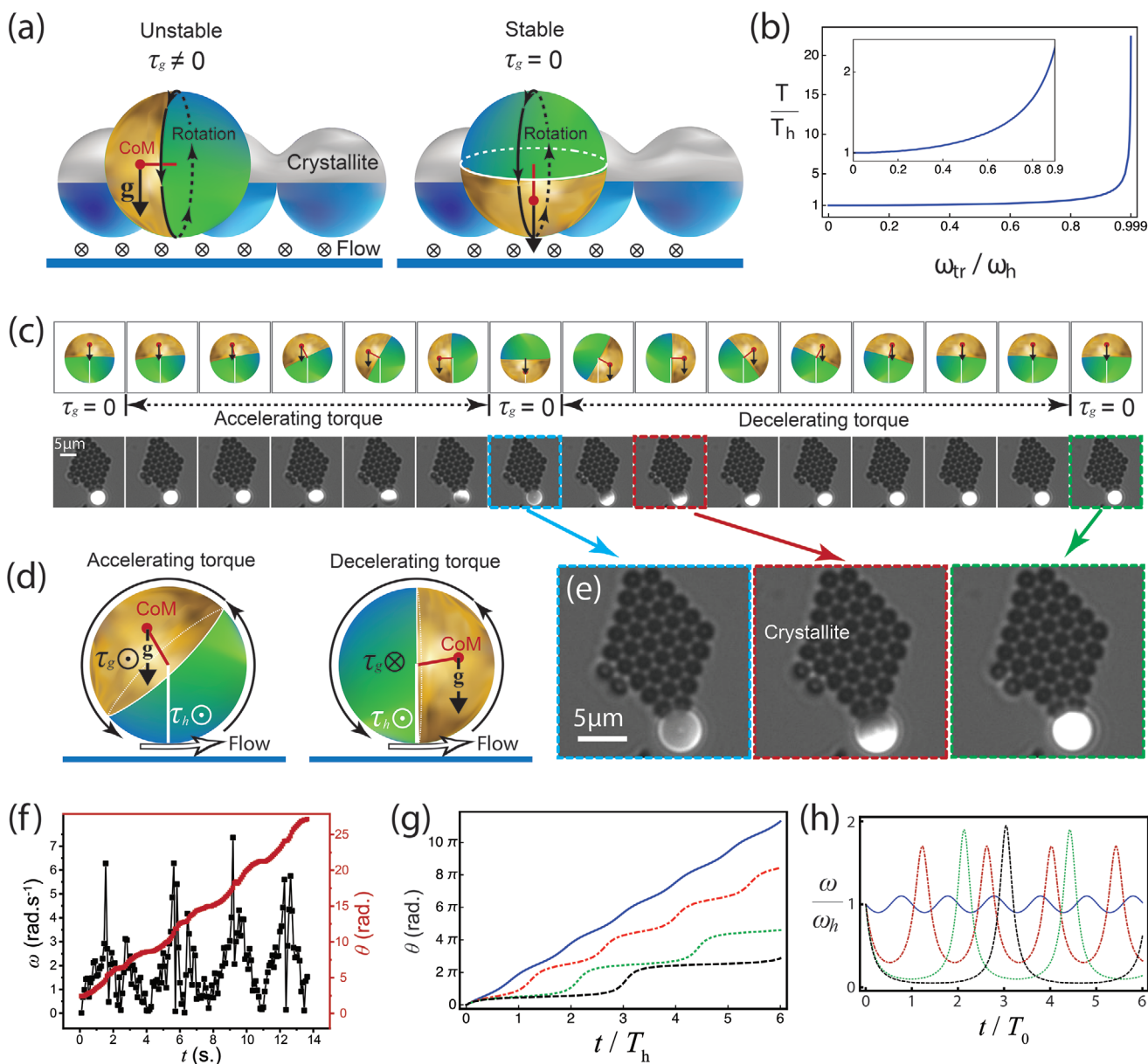
Figure 4. The effect of gravitaxis upon time-dependent dynamics. CoM in the figure refers to the center of mass of the shell. a) Schematics showing the stabilization mechanism—see main text for detailed description. b) The period of rotation T depends on the ratio of the amplitude of the gravity-induced spinning rate over the steady hydrodynamic one, ω_{tr}/ω_h. c) A series of video frames with corresponding schematics of example phases of rotation for a single cycle. The phases that correspond to τ_g and τ_h being additive, competitive, or neutral ($\tau_g = 0$) are indicated. d) Schematics showing two example phases of rotation in which the gravitational, τ_g, and flow-induced torques, τ_h add or subtract on the left- and right-hand side, respectively. e) Frames representing different orientation of the spinning particle. f) The experimental data for the dependence of frequency and angle upon time. Theoretical model for the variation of (g) orientation θ and (h) dimensionless spinning rate $\omega(t)/\omega_h$ with dimensionless time ($T_h = 2\pi/\omega_h$) for values of ω_{tr}/ω_h equal to 0.3 (solid blue), 0.7 (dotdashed red), 0.9 (dotted green), and 0.99 (dashed black). The behavior corroborates the model as depicted in (a).

(heliotropism) or the downward growth of plant root (gravitropism). We observed an analogous trend in the free Janus particles herein such that the gravity leads to self-stabilization of the spinning behavior. Gravitropic re-orientation of a free Janus particle, as shown in **Figure 4**a, renders the spinning behavior almost exclusively 1D in all of our experiments, with the two faces of the Janus sphere rotating "top-over-bottom," as presented in Figures 2d,e and 3d. Fluctuations caused by Brownian motion or by alterations in the flow field caused by,

for example, other nearby active crystallites may cause the axis of rotation to deviate away from the bisecting plane separating the two sides of Janus sphere. However, as shown in Figure 4a, the center of mass (CoM) of the shell in the Janus particle is shifted off the bisecting plane. Consequentially, gravitational torque rotates the particle such that its axis of rotation falls within, or is parallel to, the bisecting plane; thus, such behavior shows similarities to biological tropism in response to gravity. Any lateral deviations of the CoM (left-hand side of Figure 4a)

**ADVANCED
SCIENCE NEWS**

www.advancedsciencenews.com

Particle
& Particle Systems Characterization

www.particle-journal.com

are unstable and are ultimately self-corrected by the effect of gravity (right-hand side of Figure 4a).

In addition to gravitropic self-stabilizing phenomena, gravity also affects the period, T, of rotation as shown in Figure 4b. The flow field results in a hydrodynamic-induced spinning rate ω_h and the gravity-induced torque leads to an orientation-dependent transient spinning rate $\omega_{tr} \sin \theta$ as we will elaborate shortly. Using the definition of orientation θ in Figure 2d, the dimensionless spinning rate follows

$$\frac{\omega(t)}{\omega_h} = \frac{1}{\omega_h} \frac{d\theta}{dt} = 1 - \frac{\omega_{tr}}{\omega_h} \sin \theta \qquad (1)$$

which depends on the ratio of gravity-induced to hydrodynamic-induced spinning rates, ω_{tr}/ω_h. Thus, the ratio of the spinning period T over hydrodynamic period $T_h = 2\pi/\omega_h$ depends on ω_{tr}/ω_h, and as shown in Figure 2d, T/T_h diverges at $\omega_{tr}/\omega_h = 1$, and for $\omega_{tr}/\omega_h > 1$, we will have no spinning.

The instantaneous spinning rate in Equation (1) is a function of θ, and thus, time.[52] That is, the angular frequency, ω, is not constant during one period, T, of complete rotation. This effect can be seen in the series of schematics and video frames in Figure 4c in which the crystallite is made from 1.5 µm diameter SiO_2 microspheres, while the single spinning Janus particle is a polystyrene-based, fluorescent sphere of ≈3 µm diameter half-coated with 50 nm of Au. The center of mass of the polystyrene bead without the metal coating is at the center of the particle and does not lead to torque about the particle center. However, the center of mass of the shell is about three quarter the radius of the particle away from the particle center and induces torque, as demonstrated in Figure 4d. Therefore, the lowest energy configuration is with the metal cap downward toward the surface, or $\theta = 0$ as previously defined in Figure 2d.

For a free Janus particle undergoing diffusion in water, and in the absence of any active crystallite, the combination of gravitational and stochastic (Brownian) forces causes the particles' orientations to fluctuate around an average orientation $\overline{\theta} = 0$ (as shown in the Supporting Information video, which illustrates how the orientation is biased by gravity). Since the gravity effect is independent of hydrodynamic effects, gravity plays critical roles in the spinning dynamics once the crystallites are activated. The schematics in Figure 4d show two scenarios in which the gravitational torque, τ_g, either adds or subtracts to the hydrodynamic torque applied from the fluid flow, depending upon the particle's orientation. The measurements of $\omega(t)$ and $\theta(t)$ for the same particle presented in Figure 4c are plotted in Figure 4e. As expected, $\omega(t)$ peaks when the gravitational torque is maximized, around $\theta = 3\pi/2$ radians. Integrating Equation (1) results in curves for $\theta(t)$ and $\omega(t)$ in Figures 4f and 4g, respectively, as a function of ω_{tr}/ω_h. The theoretical patterns are similar to the experimental observations in Figure 4e. With increase in ω_{tr}/ω_h, the time distance (which is spinning period T) between the peaks in $\omega(t)$ increases.

3. Conclusion

To conclude, we have presented an autonomous self-assembled microstructure based on free particles and active microcrystallites. These self-assembled structures demonstrate periodic dynamics that are dominated by hydrodynamics effects, gravitational torque, and geotropic self-correction of the spinning Janus particles' orientation without any external manipulation. Our experimental results successfully corroborated with a minimal model and multiphysics simulations. To recap the model, activation in H_2O_2 generates a hydrodynamic flow field underneath and through the crystallite, which is responsible for both self-assembly and the regular spinning motion of free particles at the edge. A more comprehensive model to take into account the effects of phoretic interactions[50] and possible contributions from density driven convective flow[51] is a subject of our future studies. We will also investigate the effect of crystallite size on the dynamics of spinning particles and whether there is a critical crystallite size to see the phenomena.

The diffusiophoretic flow by an active microcrystallite may look similar to the microfluidic pumping of tracer particles by a fixed palladium patch on a gold surface using hydrazine fuels.[53] However, there is a critical fundamental difference: While the flow field is present only over the surface of a flat catalytic patch in a micropump, microcrystallites also have flow fields underneath and through the porous crystal–a necessary component required for the successful creation and self-assembly of these complex active structures. Moreover, the crystallites herein are not fixed to the surface, but are instead mobile. As such, upon activation, we often observe drifting motion, which is likely due to unequal inward flow magnitudes arriving at different edges of the crystallite, or from background convective flow (see Video V2, Supporting Information). The interplay of the multiple parameters involved in the dynamics of the autonomous microstructures provides a unique and novel architecture for designing advanced microscale systems with predictable and self-correcting performance and can be the source of inspiration for developing complex microrobots.

4. Experimental Section

In order to fabricate the Janus crystallites as well as single Janus particles, the process was started by forming monolayers of monodisperse microspheres (coefficient of variation, $CV < 3\%$) onto the polished side of Si(100) wafers via a Langmuir–Blodgett method. The particles were either polystyrene-based, dyed with a fluorophore (Polysciences, Inc., Warrington, PA) or were unfunctionalized SiO_2-based (Bangs Laboratories, Inc., Fishers, IN). Materials such as gold, platinum, and titanium dioxide (Jefferson Hills, PA) were deposited onto the monolayers using electron-beam evaporation at a background pressure of ≈10^{-5} Torr, which led to the exposed top-halves of the spheres being coated, that is, Janus spheres. Thicknesses of the deposited materials fell within the range of 50 – 200 nm. In order to ensure proper adhesion to the microspheres, ≈5 nm of titanium was deposited before the primary materials noted above.

After deposition, the Janus structures were cleaned with argon plasma (Harrick Plasma, Inc., Ithaca, NY). Note that the plasma cleaning process appears to cause photobleaching of the fluorescent dyes, but this effect did not completely destroy the fluorophores. Next, the Janus spheres and crystallites were dispersed into pure water with diluted concentrations of hydrogen peroxide (Sigma-Aldrich, St. Louis, MO) in the range 1–5% V/V. Particle dynamics was observed using an Eclipse Ti2 inverted fluorescence microscope (Nikon, Inc., Tokyo, Japan). Videos were captured of the particles spinning with a CCD camera (Thorlabs, Inc., Newton, NJ) at a frame rate of ≈10 fps in order

**ADVANCED
SCIENCE NEWS**
www.advancedsciencenews.com

Particle
& Particle Systems Characterization
www.particle-journal.com

to calculate the angular frequency. For color videos, a Leica confocal microscope (Wetzlar, Germany) system was used in the Imaging and Histology Core Facility at Northern Arizona University. The observation cell was created by cutting a hole from a square piece of double-sided tape, sandwiched between two clean coverslides, forming the bottom and top of the cell. Before sealing the cell, using a hydrophobic PAP pen, a barrier was drawn onto the bottom coverslide where the inner edge of the tape ended to prevent the fluid containing the particles from escaping the well. After, the mixture of particles, water, and hydrogen peroxide was pipetted into the cell. The scanning electron microscopy (SEM) images were obtained using a Zeiss Supra 40VP.

Simulation of Flow Pattern MDAH—Formulation of the Problem: The decomposition of fuel over the active surface of a microcrystallite results in a flux Γ_{O_2} of O_2. Under the assumption of negligible Péclet number, the equations used to obtain the oxygen concentration was decoupled from the fluid flow. At steady state, the flux of oxygen is

$$\boldsymbol{J}_{O_2} = -D_{O_2} \boldsymbol{\nabla} C_{O_2} \tag{2}$$

and the governing equation for the concentration of oxygen followed the conservation of mass equation,

$$\boldsymbol{\nabla} \cdot \boldsymbol{J}_{O_2} \propto \nabla^2 C_{O_2} = 0 \tag{3}$$

So, we need to solve the Laplace equation for C_{O_2}. Using Equation (2), the surface flux is

$$\hat{n} \cdot \boldsymbol{J}_{O_2} = -D_{O_2} \hat{n} \cdot \boldsymbol{\nabla} C_{O_2} = \Gamma_{O_2} \quad \text{on the surface of Pt} \tag{4}$$

and

$$\hat{n} \cdot \boldsymbol{J}_{O_2} = -D_{O_2} \hat{n} \cdot \boldsymbol{\nabla} C_{O_2} = 0 \quad \text{on any other surface} \tag{5}$$

On the outer boundaries of the simulation box, we impose

$$C_{O_2} = C_{O_2}^\infty \quad \text{as} \quad \boldsymbol{x} \to \infty \tag{6}$$

We model the solution as an incompressible fluid governed by the continuity equation,

$$\nabla \cdot u = 0 \tag{7}$$

and the Stokes equation

$$-\boldsymbol{\nabla} P + \eta \nabla^2 \boldsymbol{u} = 0 \tag{8}$$

The spatial gradient of the O_2 molecules resulted in a slip velocity on the surfaces

$$\boldsymbol{u}_{\text{slip}} = \mu_{\text{ph}} (\mathcal{I} - \hat{n}\hat{n}) \cdot \boldsymbol{\nabla} C_{O_2} \tag{9}$$

All the surfaces are subjected to slip velocity (9). We assumed a uniform phoretic mobility.

The hydrodynamics-induced spinning of a free particle is the result of torques applied on a particle due to diffusiophoretic flow. The velocity field over the surface of the rotating sphere is

$$\boldsymbol{u}_{\text{l}} = \boldsymbol{u}_{\text{slip}} + \boldsymbol{\omega}_h \times (x_S - x_0) \tag{10}$$

where ω_0 is the angular velocity, x_S is a point on the surface of the sphere, and x_0 is the center of the rotating particle. Since the particle is torque-free,

$$\int_{\text{free particle surface}} dS\, (x_S - x_0) \times (\sigma_H \cdot \hat{n}) = 0 \tag{11}$$

where

$$\sigma_H \cdot \hat{n} = [-P\mathcal{I} + \eta(\boldsymbol{\nabla}\boldsymbol{u} + (\boldsymbol{\nabla}\boldsymbol{u})^T)] \cdot \hat{n} \tag{12}$$

is the traction.

Finite Element Simulation: We first start with making the equations dimensionless. We work in units of small-particle radius a for length, far-field O_2 concentration $C_{O_2}^\infty$ for concentration, $J^* = D_{O_2} C_{O_2}^\infty$ for flux, $U^* = \mu_{\text{ph}} C_{O_2}^\infty / a$ for fluid velocity, and $P^* = \eta\, U^*/a$ for pressure, and we use the notation $\tilde{\ }$ for dimensionless quantities. The concentration of O_2 is governed by the Laplace equation

$$\tilde{\nabla}^2 \tilde{C}_{O_2} = 0 \tag{13}$$

and boundary conditions

$$-\hat{n} \cdot \tilde{\nabla}\tilde{C}_{O_2} = \tilde{\Gamma}_{O_2} \equiv \frac{a\Gamma_{O_2}}{D_{O_2} C_{O_2}^\infty} \quad \text{on the surface of Pt} \tag{14}$$

$$\tilde{C}_{O_2} = 1 \quad \text{as} \quad \tilde{\boldsymbol{x}} \to \infty \tag{15}$$

For fluid flow we have the governing equations

$$\tilde{\nabla} \cdot \tilde{\boldsymbol{u}} = 0 \tag{16}$$

$$\tilde{\nabla}\tilde{P} + \tilde{\nabla}^2 \tilde{\boldsymbol{u}} = 0 \tag{17}$$

with slip velocity

$$\tilde{\boldsymbol{u}}_{\text{slip}} = (\mathcal{J} - \hat{n}\hat{n}) \cdot \tilde{\nabla}\tilde{C}_{O_2}. \tag{18}$$

Therefore, there is only one parameter that controls the dimensionless equations, that is, $\tilde{\Gamma}_{O_2} \equiv a\Gamma_{O_2}/(D_{O_2} C_{O_2}^\infty)$.

In order to obtain the $\tilde{\omega}_h = \omega_h a/U^*$ for a given $\tilde{\Gamma}_{O_2}$, we guess a set of values for $\tilde{\omega}_h$, run the simulations and by interpolation we find a value of $\tilde{\omega}_h$, for which the torque is zero. Figure 3f shows the results of the COMSOL simulations for three values of free particle radius R compared to the radius a of a small-particle in the microcrystallite.

Supporting Information

Supporting Information is available from the Wiley Online Library or from the author.

Acknowledgements

Conflict of Interest

The authors declare no conflict of interest.

Data Availability Statement

The data that support the findings of this study are available on request from the corresponding author. The data are not publicly available due to privacy or ethical restrictions.

[1] S. Sánchez, L. Soler, J. Katuri, *Angew. Chem. Int. Ed.* **2015**, *54*, 1414.

[2] J. Li, W. Gao, R. Dong, A. Pei, S. Sattayasamitsathit, J. Wang, *Nat. Commun.* **2014**, *5*, 5026.

[3] V. Yadav, W. Duan, P. J. Butler, A. Sen, *Annu. Rev. Biophys.* **2015**, *44*, 77.

[4] P. Fischer, *Nat. Phys.* **2018**, *14*, 1072.

[5] J. G. Gibbs, S. Sarkar, A. Leeth Holterhoff, M. Li, J. Castañeda, J. Toller, *Adv. Mater. Interfaces* **2019**, *6*, 1801894.

[6] J. Simmchen, J. Katuri, W. E. Uspal, M. N. Popescu, M. Tasinkevych, S. Sánchez, *Nat. Commun.* **2016**, *7*, 10598.

[7] A. Nourhani, P. E. Lammert, *Phys. Rev. Lett.* **2016**, *116*, 178302.

[8] A. Nourhani, V. H. Crespi, P. E. Lammert, *Phys. Rev. E* **2015**, *91*, 062303.

[9] J. Elgeti, R. G. Winkler, G. Gompper, *Rep. Prog. Phys.* **2015**, *78*, 056601.

[10] M. Popescu, W. Uspal, Z. Eskandari, M. Tasinkevych, S. Dietrich, *Eur. Phys. J. E* **2018**, *41*, 145.

[11] W. F. Paxton, K. C. Kistler, C. C. Olmeda, A. Sen, S. K. St. Angelo, Y. Cao, T. E. Mallouk, P. E. Lammert, V. H. Crespi, *J. Am. Chem. Soc.* **2004**, *126*, 13424.

[12] A. A. Solovev, Y. Mei, E. Bermúdez Ureña, G. Huang, O. G. Schmidt, *Small* **2009**, *5*, 1688.

[13] H. Ke, S. Ye, R. L. Carroll, K. Showalter, *J. Phys. Chem. A* **2010**, *114*, 5462.

[14] S. Das, A. Garg, A. I. Campbell, J. Howse, A. Sen, D. Velegol, R. Golestanian, S. J. Ebbens, *Nat. Commun.* **2015**, *6*, 8999.

[15] U. Choudhury, A. V. Straube, P. Fischer, J. G. Gibbs, F. Höfling, *New J. Phys.* **2017**, *19*, 125010.

[16] É. O'Neel-Judy, D. Nicholls, J. Castañeda, J. G. Gibbs, *Small* **2018**, *14*, 1801860.

[17] J. G. Gibbs, S. Kothari, D. Saintillan, Y.-P. Zhao, *Nano Lett.* **2011**, *11*, 2543.

[18] M. Kaynak, A. Ozcelik, A. Nourhani, P. E. Lammert, V. H. Crespi, T. J. Huang, *Lab. Chip.* **2017**, *17*, 395.

[19] F. Soto, M. A. Lopez-Ramirez, I. Jeerapan, B. E.-F. de Avila, R. K. Mishra, X. Lu, I. Chai, C. Chen, D. Kupor, A. Nourhani, J. Wang, *Adv. Funct. Mater.* **2019**, *29*, 1900658.

[20] F. Zhang, R. Mundaca-Uribe, H. Gong, B. Esteban-Fernández de Ávila, M. Beltrán-Gastélum, E. Karshalev, A. Nourhani, Y. Tong, B. Nguyen, M. Gallot, Y. Zhang, L. Zhang, J. Wang, *Adv. Mater.* **2019**, *31*, 1901828.

[21] S. Palagi, P. Fischer, *Nat. Rev. Mater.* **2018**, *3*, 113.

[22] H. Xu, M. Medina-Sánchez, V. Magdanz, L. Schwarz, F. Hebenstreit, O. G. Schmidt, *ACS Nano* **2017**, *12*, 327.

[23] M. M. Stanton, J. Simmchen, X. Ma, A. Miguel-López, S. Sánchez, *Adv. Mater. Interfaces* **2016**, *3*, 1500505.

[24] Y. Alapan, O. Yasa, B. Yigit, I. C. Yasa, P. Erkoc, M. Sitti, *Annu. Rev. Control, Robotics, and Autonomous Sys.* **2019**, *2*, 205.

[25] F. Ginot, I. Theurkauff, D. Levis, C. Ybert, L. Bocquet, L. Berthier, C. Cottin-Bizonne, *Phys. Rev. X* **2015**, *5*, 011004.

[26] É. Fodor, M. C. Marchetti, *Physica A* **2018**, *504*, 106.

[27] W. Gao, X. Feng, A. Pei, Y. Gu, J. Li, J. Wang, *Nanoscale* **2013**, *5*, 4696.

[28] B. Jurado-Sánchez, J. Wang, *Environ. Sci.: Nano* **2018**, *5*, 1530.

[29] A. M. Boymelgreen, T. Balli, T. Miloh, G. Yossifon, *Nat. Commun.* **2018**, *9*, 760.

[30] S. Ramananarivo, E. Ducrot, J. Palacci, *Nat. Commun* **2019**, *10*, 3380.

[31] F. Soto, E. Karshalev, F. Zhang, B. Esteban Fernandez de Avila, A. Nourhani, J. Wang, *Chem. Rev.* **2021**, https://doi.org/10.1021/acs.chemrev.0c00999.

[32] A. Nourhani, D. Brown, N. Pletzer, J. G. Gibbs, *Adv. Mater.* **2017**, *29*, 1703910.

[33] J. N. Johnson, A. Nourhani, R. Peralta, C. McDonald, B. Thiesing, C. J. Mann, P. E. Lammert, J. G. Gibbs, *Phys. Rev. E* **2017**, *95*, 042609.

[34] A. Zöttl, H. Stark, *Phys. Rev. Lett.* **2014**, *112*, 118101.

[35] W. Gao, A. Pei, X. Feng, C. Hennessy, J. Wang, *J. Am. Chem. Soc.* **2013**, *135*, 998.

[36] P. Bayati, A. Najafi, *J. Chem. Phys.* **2016**, *144*, 134901.

[37] F. Ginot, I. Theurkauff, F. Detcheverry, C. Ybert, C. Cottin-Bizonne, *Nat. Commun.* **2018**, *9*, 696.

[38] A. Nourhani, S. J. Ebbens, J. G. Gibbs, P. E. Lammert, *Phys. Rev. E* **2016**, *94*, 030601.

[39] A. Nourhani, P. E. Lammert, A. Borhan, V. H. Crespi, *Phys. Rev. E* **2014**, *89*, 062304.

[40] A. Nourhani, V. H. Crespi, P. E. Lammert, *Phys. Rev. E* **2014**, *90*, 062304.

[41] J. R. Howse, R. A. Jones, A. J. Ryan, T. Gough, R. Vafabakhsh, R. Golestanian, *Phys. Rev. Lett.* **2007**, *99*, 048102.

[42] A. Nourhani, D. Saintillan, *Phys. Rev. E* **2021**, *103*, L040601.

[43] I. S. Aranson, *C. R. Phys.* **2013**, *14*, 518.

[44] W. Wang, W. Duan, A. Sen, T. E. Mallouk, *Proc. Natl. Acad. Sci.* **2013**, *110*, 17744.

[45] E. Pinçe, S. K. Velu, A. Callegari, P. Elahi, S. Gigan, G. Volpe, G. Volpe, *Nat. Commun.* **2016**, *7*, 10907.

[46] U. Choudhury, D. P. Singh, T. Qiu, P. Fischer, *Adv. Mater.* **2019**, *31*, 1807382.

[47] A. Walther, A. H. Muller, *Chem. Rev.* **2013**, *113*, 5194.

[48] A. I. Campbell, S. J. Ebbens, P. Illien, R. Golestanian, *Nat. Commun.* **2019**, *10*, 3952.

[49] D. McKee, *J. Catal.* **1969**, *14*, 355.

[50] D. P. Singh, U. Choudhury, P. Fischer, A. G. Mark, *Adv. Mater.* **2017**, *29*, 1701328.

[51] O. E. Shklyaev, H. Shum, V. V. Yashin, A. C. Balazs, *Langmuir* **2017**, *33*, 7873.

[52] J. Katuri, W. E. Uspal, J. Simmchen, A. Miguel-López, S. Sánchez, *Sci. Adv.* **2018**, *4*, eaao1755.

[53] M. E. Ibele, Y. Wang, T. R. Kline, T. E. Mallouk, A. Sen, *J. Am. Chem. Soc.* **2007**, *129*, 7762.